Disentangled UHMWPE@silica powders for potential use in power bed fusion based additive manufacturing

Wencke, Yannick L.; Luinstra, Gerrit A.; Duchateau, Rob; Proes, Friedrich; Imgrund, Philipp; Evenson, Jonathan S.; Emmelmann, Claus

Published in:
European Polymer Journal

DOI:
10.1016/j.eurpolymj.2021.110936

European Polymer Journal 163 (2022) 110936

Contents lists available at ScienceDirect

European Polymer Journal

journal homepage: www.elsevier.com/locate/europolj

Disentangled UHMWPE@silica powders for potential use in power bed fusion based additive manufacturing

Yannick L. Wencke [a], Gerrit A. Luinstra [a,*], Rob Duchateau [b,c], Friedrich Proes [d], Philipp Imgrund [d], Jonathan S. Evenson [d], Claus Emmelmann [d]

[a] Institute for Technical and Macromolecular Chemistry, Bundesstraße 45, 20146 Hamburg, Germany
[b] SABIC Technology & Innovation, STC Geleen, Urmonderbaan 22, Geleen, the Netherlands
[c] Chemical Product Engineering, Department of Chemical Engineering, University of Groningen, Nijenborgh 4, 9747 AG Groningen, the Netherlands
[d] Fraunhofer-Einrichtung für Additive Produktionstechnologien IAPT, Am Schleusengraben 14, 21029 Hamburg, Germany

ARTICLE INFO

Keywords:
Disentangled ultrahigh molecular weight polyethylene
dUHMWPE
Bisimine pyridine iron catalyst
Heat pressed plate
Mechanical properties
Powder properties
Supported olefin polymerization catalyst
Powder bed fusion

ABSTRACT

Disentangled ultrahigh molecular weight polyethylene dUHMWPE (Mw ~ 2.10^6 Da) particles in a reactor blend with HDPE are catalytically prepared from ethylene, mediated by a new catalyst from N,N'-(2,6-pyridinediyl diethylidyne) bis[2,6-di-3-propenyl-benzenamine] iron dichloride and triethyl aluminum. These particles could be laser sintered, but not automatically processed in an SLS machine. The same catalyst supported on microsilica particles gives access to composite dUHMWPE@silica particle powder with particle sizes below 200 μm. Testing bars prepared by heat pressing have an Emod of 150 MPa, an elongation at break at 450 % and an ultimate strength of 39 ± 11 MPa. A SEM image indicates a silica induced crystallization into pseudo spherulites of 500 μm size. The dUHMWPE@silica composite particles have an fcc flowability value of 3.4 in a ring shear tester, and a low density of 150 kg.m^{-3}. Additivation with nanosilica powder (1 wt%) and carbon black (0.25 wt%) allowed to process the composite in an SLS machine. The printed parts showed severe caking, but also a complete welding of the powder, albeit with voids on account of the low particle density.

1. Introduction

Linear polyethylene with ultrahigh molecular weight (>10^6 Da) is notoriously hard to process when it is entangled. The small critical molecular mass of polyethylene gives rise to an unusual high number of entanglements in UHMWPE, which results in exceedingly long relaxation times. The processing is only economical from gels or by compression molding [1]. The latter also leads to the breakdown of chains. The property profile in terms of chemical resistance and mechanics on the other hand, brings UHMWPE in a class of its own when it comes to tensile strength, or friction, impact and fatigue resistance. It also is biocompatible and used in e.g. artificial joints as hip and knee replacements [2,3].

Processing of UHMWPE in 3D printing as an additional procedure bears the promise of getting to the mechanically superior built parts in any form or shape [4–6]. The additive manufacturing (AM) based on laser sintering of powders, PBF/LB/P (powder bed fusion/laser bed/polymer, aka SLS), probably is the most versatile technology in that regard. The prerequisites for suitable powders are, however, quite extensive and originate from the three designated steps of AM based on PBF, powder recoating, energy input for local melting and powder coalescence followed by solidification [7,8]. Two triad relationships have been introduced to break down the requirements: one for printability and one for printed parts. The printability triad comprises the chemical and morphological properties of the polymer powder that enable processing in an SLS machine. The printed part triad concerns the printing process, melting and solidification together with the properties of the manufactured parts. The final properties of a built part are set within the attainable profile of the material, which would be excellent for UHMWPE and its blends with other polyethylenes [9].

The printability of the powder requires the recoater to reach a dense and uniform layer. Powders with a substantial spherical shape with a smooth surface and an average particle size in range of 10 to 120 μm with a narrow distribution are favorable in that regard. They should have a reasonable powder flowability (e.g. when characterized in ring shear tester by an fcc of 3 or more). Fusion of the powder by laser light is possible when the powder absorbs the relevant wavelengths. The absorbance is also relevant for diminishing energy scattering, leading to

* Corresponding author.
E-mail address: Luinstra@chemie.uni-hamburg.de (G.A. Luinstra).

https://doi.org/10.1016/j.eurpolymj.2021.110936
Received 31 August 2021; Received in revised form 29 November 2021; Accepted 5 December 2021
Available online 10 December 2021

a loss of dimensional accuracy of the built part: part of the scattered energy may melt powder outside the scanning range, leading to caking [10].

The powder should have a sinter window in the context of selective laser sintering (SLS), i.e. a workable difference (30 °C) between the onsets of crystallization and melting [7]. The laser sintering should be carried out at a bed temperature within the sinter window. The powder is locally molten by the laser above the crystallization temperature: crystallization best takes only place after solidification once the powder bed is cooled down after completion of the printing job. This procedure should minimize curling and warpage, severe disorders that can result if a uniform crystallization cannot be achieved. In addition, the laser-molten polymer should have the possibility to flow, contacting neighboring particles and underlying layers to form a solid built part, free from voids. The built parts then may reach the level of mechanical strength of the bulk material. The formation of voids is, however, not easy to prevent, i.e. after a first contact of the particle's molten surface, surface tension and capillary forces may be too weak to overcome the viscoelastic resilience of the material against flow [11]. The fusion process is then frozen in the initial state of necking particles, giving porous objects.

The particles favorably have a density close to that of the bulk and have a shape that allows a dense packing to further avoid the presence of voids in the printed part. For UHMWPE, the corresponding powder GUR 2122 from Celanese has been thoroughly characterized in that regard [6]. The particles have an irregular shape, consisting of strands of polymer, and the sinter result is apt for improvement [5]. The sintered parts were porous with a relative density of little over one third with respect to the typical density of PE [12,13].

The option of using disentangled dUHMWPE in AM along SLS is one of generating a low(er) viscous melt and a high strength part as melting dUHMWPE goes along with the formation of entanglements [14,15]. In addition, the crystallization can be modified by the presence of polyethylene waxes, allowing to take influence on curling and warpage [16]. Thermal sintering of UHMWPE thus could lead to superior built parts [17]. The preparation of dUHMWPE is relatively straightforward. Several catalyst systems are reported that do not readily chain terminate and yield UHMWPE in several states of disentanglement [1,18–29]. It is an interplay of catalyst concentration and with that polymer chain concentration, relative polymerization and crystallization rate. The polymerization should effectively be carried out in a way that the action of one catalyst center is not interfered by other catalyst centers, and a newly formed chain can crystallize into individual lamellae without getting entangled with other polymer chains. This can be achieved by dilution in case of homogenous catalysis or by compartmentalization of sites in a supported catalyst [1,24], like in channels of zeolites [30], in droplets of a two-phase system [31], introduction of spacer in form of polyhedral oligomeric silsesquioxane to keep polymer crystals apart [32]. Effectively, also other types of linear polyethylenes directly prepared by polymerization below the melting point may be in a partial disentangled state [32–35]. Most of the entanglements are formed in an early state of polymer formation, when the chain are short and mobile; also classical Ziegler-Natta catalysts can give kind of dUHMWPE when run at relatively low ethylene pressure [36].

UHMWPE can also be kept in a processable state in reactor blends, in particular polyethylene blends prepared by the action of two or more catalysts. A few combinations of homogeneous catalysts with different metals were found useful in that regard [9]. The catalysts were e.g. supported on disintegrating supports, leading to particles in a mm size, favorable for handling in standard slurry or gas phase reactors [33,37]. The resulting products in part are rather porous, which is also unfavorable for application in AM. The choice of support allows to take influence on the morphology of polyethylene particle, i.e. the support may act as a template for the preparation of polyethylene particles [38]. The preparation of smaller and denser particles is feasible starting from integer silica particles. Very recently the preparation of nascent (near) disentangled UHMPE particles with a mean size of 200 μm was reported [39]. The particles were not spherical as no corresponding template was used. It shows, however, that UHMWPE formed in a living polymerization will be in a substantial disentangled state.

We thus set out to prepare dUHMWPE@silica particles in the range below 200 μm by a direct synthesis from ethylene using a silica supported single site iron catalyst. A template-directed particle preparation seemed an attractive method of getting to AM suitable UHMWPE basis. dUHMWPE in bulk cannot be thermoplastically processed without losing the disentangled state, and corresponding particles cannot be prepared from the melt. As a consequence, dUHMWPE is also not available in bulk for milling. The envisioned route of preparation for particles was using a slurry polymerization process with toluene as the medium. Such a procedure would optionally allow incorporating additives for laser light absorption and stabilizers (UV, temperature) in an advanced stage. In this way, an option for preparing UHMWPE built parts by thermoplastic processing or AM with adjustable features would become available.

Bisimine-pyridine iron dichloride complexes (BIP $FeCl_2$) were chosen as catalyst precursors. The N,N,N ligand frame of bisimine pyridines is easily modified and has been a versatile basis for the preparation of a multitude of iron(II) dichloride polymerization and other catalysts [40,41]. The choice of ligand allows to tune the complex in combination with an activator from an ethylene oligomerization catalyst to a system generating high molecular weight polyethylene. The catalyst system can readily be supported on silica and other carriers keeping its high activity, and is still subject of recent developments [42–48]. The family of iron catalysts would allow to choose a combination for the preparation of a blend of polyethylenes, as they have various modes of polyethylene formation. It thus seems useful to extent this technology, as it has been shown that PE prepared on a support can be tuned in their flow properties by using a combination of catalysts [33,49–52].

2. Experimental

2.1. Materials

All manipulation of air- and/or moisture-sensitive compounds was carried out under a dry nitrogen atmosphere using standard Schlenk-techniques. Micro-sized silica in form of Perkasil 300 KS was generously supplied by W. R. Grace and Company. UHMWPE was a gift from Celanese Corporation. Aniline was purchased from SIAL and used without further purification. Allyl bromide and sodium carbonate were purchased from Merck. Magnesium sulfate was purchased from Grüssing. Xylene was purchased from Kraft. Absolute diethyl ether, BF_3 etherate solution, *para*-toluenesulfonic acid, 2,6-diacetylpyridine, iron dichloride, methanol, 1-butanol and ethanol were purchased from Sigma-Aldrich. All these compounds were used without further purification. $CDCl_3$ was purchased from Deutero GmbH.

2.2. Synthesis of 2,6–Bis[1–(2,6-dipropen-3-yl phenylimino) ethyl] pyridine

2,6-Diacetylpyridine (0.17 g, 1.0 mmol), 2,6–diallyl aniline (0.99 g, 5.7 mmol, 5.7 equiv.), *p*-toluene sulfonic acid (56 mg, 280 μmol, 28 mol %) and ~ 1 g molecular sieve type 4 Å were suspended in 6 mL absolute toluene under an nitrogen atmosphere. The reaction mixture was refluxed for 20 h. After cooling to room temperature, the solution was reduced *in vacuo* to 3 mL and 100 mL of methanol were added. The mixture was held at –18 °C for 48 h. The precipitated crystals were collected on a filter frit and washed with methanol. Yield: 0.17 g, 360 μmol, 36 %.

^{1}H NMR (600 MHz, $CDCl_3$): δ [ppm] = 8.51 (d, J = 7.8 Hz, 1H, H-2), 7.94 (t, J = 7.8 Hz, 1H, H-3), 7.15 (d, J = 7.6 Hz, 4H, H-8), 7.06 (d, J = 7.6 Hz, 2H, H-9), 5.94 – 5.86 (m, 4H, H-11), 5.03– 4.97 (m, 8H, H-12), 3.18 (ddd, J = 22.9, 15.5, 6.7 Hz, 8H, H-10), 2.25 (s, 6H, H-5).

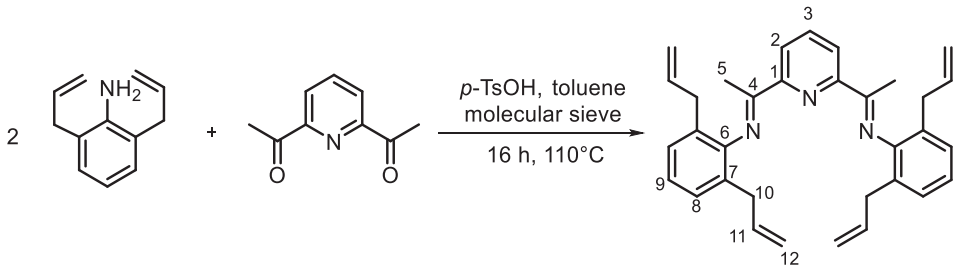

Scheme 1. Synthesis of the ligand.

^{13}C NMR (151 MHz, $CDCl_3$): δ [ppm] = 136.9 (C-3),136.5 (C-11), 135.9 (C-9), 128.5 (C-4), 128.0 (C-6), 127.6 (C-8), 127.6 (C-2), 123.6 (C-1), 122.7 (C-7), 115.9 (C-12), 36.1 (C-10), 17.4 (C-5) (assignments are in Scheme 1).

2.3. Synthesis of 2,6–Bis[1–(2,6-dipropenylphenylimino)ethyl]pyridine iron(II) dichloride

Iron(II) dichloride (27.8 mg, 219 μmol) was dissolved in 4 mL absolute *n*-butanol at room temperature under an nitrogen blanket. 2,6-bis [1-(2,6-diallylphenylimino)ethyl]pyridine (53.1 mg, 112 μmol, 0.5 equiv.) was added. The yellow solution turned instantaneous blue and a blue powder precipitated. 3 mL of absolute diethyl ether was added to the reaction mixture and the blue powder was collected on a filter frit. The residue was dried *in vacuo* to give a dark blue solid. Yield: 47.7 mg, 71 %, 79 μmol. **^{1}H NMR** (400 MHz, $CDCl_3$, paramagnetic): δ [ppm] = 78.65, 48.63, 15.27, 10.46, 1.82, 0.90, –1.32, –27.36. **ESI-MS:** *m/z* = 564.19 ([M−Cl]), 474.30 ([M - $FeCl_2$]). **MALDI-MS:** *m/z* = 599.144 ([M]), 564.176 ([M - Cl)

2.4. Microsized separated silica particles

Perkasil 300 KS was dispersed in water by ultrasound impact. Typically, 22.5 g of Perkasil were added to 277.5 mL of deionized water. The dispersion was subjected 3 times to 10 min ultrasonic impact with a Sonopuls 2070 of the company Bandelin equipped with a V70T Sonotrode head at 80 % amplitude. Subsequent spray drying was performed on a Minispray Dryer 290 with an inert loop B-295 of the company Büchi. It was executed with the aspirator at 80%, the pump at 40 % and the pressurized air at 30 % of maximum capacity. The inlet temperature was 180 °C and the outlet temperature 77 °C.

2.5. Catalyst support

Spray dried silica (1 g) was dried in a dynamic vacuum at 150 °C for 2.5 h. Subsequently, in an evacuated Schlenk vial the desired amount of precatalyst **1** suspended in dry toluene and dry dichloromethane were added (typically 2 mL of 2.4 mM **1** in toluene, 4 mL of dichloromethane). The blue solution was transferred to the silica and mixed using a laboratory mixer. The resulting slurry evaporated to dryness until a light blue, free flowing powder was received.

2.6. Ethylene polymerization

Polymerizations were performed within a Büchi miniplant reactor with supply of solvent, gases/vacuum and olefins. A 1 L glass reactor was used in this study, connected to the ethylene supply by a massflow controller. Toluene for polymerizations was supplied from Merck and purified by distillation and passing through columns filled with molecular sieve (4 Å) and BASF catalyst R3-11/G. Ethylene was purchased from Westfalen AG and was purified by passing through columns filled with molecular sieve (4 Å) and BASF catalyst R3-11/G. Triethyl aluminum (TEA) was purchased as a 25 wt% solution in toluene from Sigma-Aldrich and used as received. MAO was purchased from Crompton as a 10 % solution in toluene and used as received.

Polymerization was performed by filling the reactor with 600 mL of toluene, adding cocatalyst by syringe (MAO to a level of 2.8 mmol/L^{-1} or TEA to 3.0 mmol.L^{-1}). The solvent was saturated with ethylene gas (addition via the gas phase) to a constant pressure of 3 bars at reaction temperature. Subsequently catalyst (support/non-supported) was added as a suspension in 6 mL of toluene. After reaching the preset reaction time, the excess ethylene was discharged and the reaction was quenched by the addition of small aliquots (5 – 20 mL) of ethanol. The resulting slurry was mixed with ~ 1.5 L of ethanol and the residue collected and filtered. The white powder was dried *in vacuo* at 40 °C. The silica content was calculated from the isolated yield and the amount of silica used, assuming a complete incorporation.

2.7. Powder addition

The synthesized polyethylene particles were mixed with carbon black Ketjenblack EC 300 J (Weber und Schaer, Hamburg, Hamburg, Germany) and additionally with silicon dioxide nanoparticles (Ionic Liquids Technologies GmbH, Heilbronn, Baden-Württemberg, Germany). Mixing was performed separately for each additive, using a Speedmixer DAC 400 (Hauschild & Co KG, Hamm, North Rhine-Westphalia, Germany), switching between a cooling step, where the mixing container is cooled with ice water, and a mixing step with 2500 rpm for one minute, for a total of five cycles for each additive.

2.8. Methods

NMR-data was obtained using a Bruker AVANCEIII HD 400 MHz spectrometer. 1–5 mg of each sample were dissolved in 0.7 mL of water and acid free $CDCl_3$ and measured at room temperature. SEM images were obtained on a LEO 1525 Gemini scanning electron microscope after coating with carbon. Samples were coated with carbon using a Leica ACE 600 (both: Wetzlar, Hesse, Germany). Micrographs were recorded with an acceleration voltage of 5 kV.

High temperature size exclusion chromatography for the determination of the molecular weight distributions were executed using a PL-GPC-220 of the company Agilent. The instrument was equipped with a refractive index detector and 1,2,4-trichloro benzene was used as solvent. Measurements were executed at 135 °C and evaluated using a polystyrene calibration. The results of SEC experiments were transformed to (close to) absolute numbers by an universal calibration procedure using the Kuhn-Mark-Houwink-Sakurada equation [53].

Melting and crystallization of the polymer composites was investigated using a DSC1 of the company Mettler Toledo (Columbus, Ohio, United States). Standard non-isothermal crystallization experiments were executed for all samples by a heating from 25 °C to 180 °C at a heating rate of 10 K·min^{-1}. The sample was held at 180 °C for 5 min and then cooled to 25 °C with a cooling rate of 10 K min^{-1}. After holding the sample at this temperature, the sample was subjected to a second heating and cooling cycle with the same parameters as above. All experiments were executed in an inert nitrogen atmosphere.

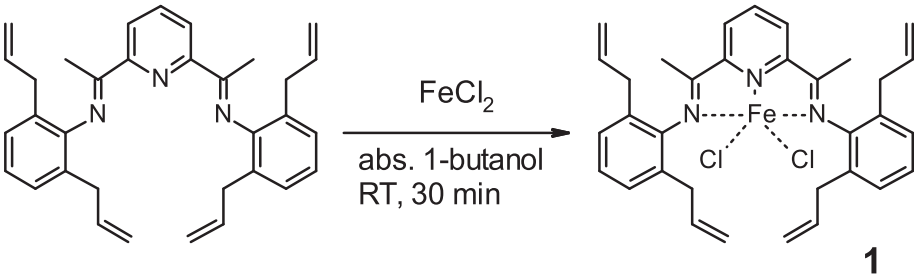

Scheme 2. Preparation and structure of the precatalyst **1**.

Annealing experiments were performed according to an adapted procedure [54]. Samples were heated close to the melting range of the material (135.6 °C/136 °C) and left to anneal at this temperature for a set amount of time. After this annealing step, the sample was cooled down to 50 °C with 10 K.min^{-1} and held at this temperature for 5 min. The protocol then consists of a heating step to 160 °C with a heating rate of 10 K.min^{-1}. After holding this temperature for 5 min the cooling and heating step were repeated once again. All experiments were executed in an inert nitrogen atmosphere.

Heat sintering was performed in mold of 100*100*1 mm^3. The powder was heated to 200 °C while applying a pressure of 200 bars. After 10 min of pressing, the mold was allowed to slowly cool to room temperature. Tensile test specimens derived from DIN EN ISO 527-5A were prepared from a heat pressed plate by die cutting. Tensile testing was performed subsequently on a Zwicki-Line Z1.0 of the company ZwickRoell (Ulm, Baden-Württemberg, Germany) with 1 kN force transducer and a crosshead speed of 50 mm.min^{-1} and at 23 °C. Samples were kept at that temperature and under the exclusion of moisture prior to measurement.

Particle size and distribution of the polymer powders and composites were measured on a HELOS KR laser diffraction sensor equipped with a RODOS/GRADIS dry dispersion setup of the company Sympatec (Clausthal-Zellerfeld, Lower Saxony, Germany). Particle roundness was determined by a dynamic image analysis according to ISO 13322–2 with a Camsizer XT of the company Retsch. (Haan, North-Rhine-Westfalia, Germany). Powder flowabillity measurements were executed on a ring-shear-tester RST-XS.s of the company Dietmar Schulze (Wolfenbüttel, Lower Saxony, Germany). A sample of 20 g was placed inside the ring shear tester and subjected to a pressure of 500 Pa. Measurements were subsequently performed at 75 Pa intervals lower until to 200 Pa.

Rheological measurements were performed on polymer samples thermally stabilized with Irganox 1010 [54]. Thus, Irganox 1010 was dissolved in acetone and polymer particles were added to give a suspension. The solvent was subsequently removed *in vacuo* until a dry polymer powder resulted with 0.5 wt% Irganox 1010. Discs of 25 mm in diameter were prepared by compressing 1 g of polymer powder in a hot press at 200 bars of pressure and 125 °C. The received discs were subsequently heated in an AR 2000 (Texas Instruments) rheometer to 160 °C at zero force. The time sweep experiment was executed under constant axial force of 4 N, an angular frequency of 10 rad/s and a strain of 0.2 %.

2.9. Powder bed Fusion.

A reduced building chamber, housed inside a commercial PBF machine (EOS P390), was designed and built to allow the testing of smaller amounts of material [55]. Several issues had to be resolved, such as correlating the set point temperature and the actual temperature on the powder surface, adjusting the gap distance between parts so no powder leakages occur and insulating/heating the build chamber. Laser parameters used were a laser power of 36 W, a scanning speed of 1500 mm.s^{-1}, and a hatch distance of 0.15 mm. The temperatures set were 122.5 °C in the process chamber and 120 °C in the removal chamber.

3. Results and discussion

3.1. Catalyst synthesis and product characterization

A serendipitous finding led to the discovery of a BIP $FeCl_2$ catalyst for the synthesis of dUHMWPE. The complex **1** with the ligand N,N'-(2,6-pyridinediyldiethylidyne) bis[2,6-di-2-propenyl] benzenamine was prepared in the context of enhancing the solubility of the complexes. The ligand was originally chosen as a precursor for further derivatives. The propenyl benzenamine is readily available from aniline and allyl bromide after N-addition and an aza-Claisen rearrangement [56]. A standard condensation with 2,6-diacetyl pyridine gives the final ligand, and complexation to iron dichloride gives the usual blue precatalyst **1** (Scheme 2). The complex is reasonably stable in dry air, and can be handled just like standard BIP $FeCl_2$ catalysts without special precautions.

Polymerization of ethylene by **1** can be achieved in toluene solvent after activation with triethyl aluminum (TEA) below room temperature. Surprisingly, the complex cannot be activated with methyl aluminoxane (MAO) for ethylene polymerization at those temperatures in a reasonable time frame. No polymerization activity was found over a period of 30 min at 0 °C at a concentration of 2.4 μmol.L^{-1} and concentrations of MAO between 0.28 mmol.L^{-1} and 2.8 mmol.L^{-1} (Table 1). This low temperature was chosen for the lower swelling of the polymeric product. Typical BIP $FeCl_2$ complexes like those based on ligands prepared from ortho alkyl substituted anilines become active ethylene polymerization catalysts in combination with MAO at such temperatures [57]. The expected color change from blue to orange did also not occur. Most of the BIP $FeCl_2$ complexes show this color change directly after contact with MAO. Instead, a color change to brown/green is observed, only at higher temperatures (40 °C) the complex turns red–orange (in a period of

Table 1
Ethylene polymerization by precatalyst **1** in combination with TEA.

entry	cocatalyst	mmol.L^{-1}	time [min]	yield [g]	activity [t.(mol bar h)$^{-1}$]	M_w (SEC) [10^6 g.mol^{-1}]	PDI
1	MAO	0.28	30	–			
2	MAO	2.8	30	–			
3	TEA	3	30	7.68	3.6	2.87	47
4	TEA	3	7.5	1.59	2.9	2.14	126

Reaction conditions: 0 °C, 2.4 μmol.L^{-1} of **1**, 600 mL of toluene, 3 bar of ethylene, 500 RPM.

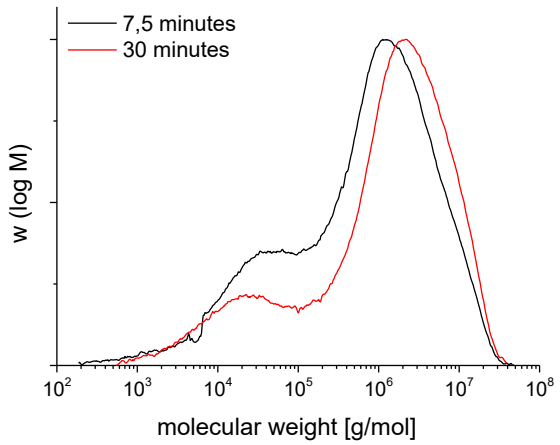

Fig. 1. Molecular weight distribution of the action of precatalyst **1** with TEA.

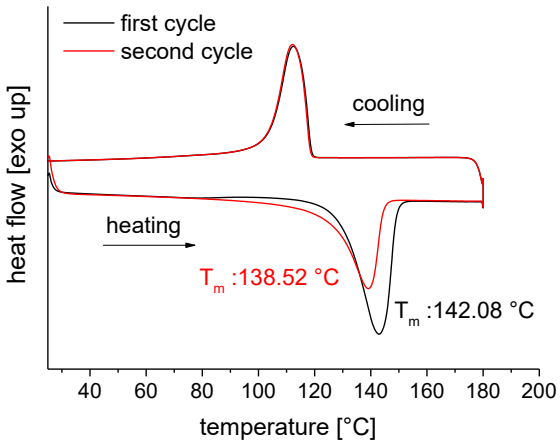

Fig. 2. DSC Measurement of maiden dUHMWPE/HDPE blend (10 °C.min^{-1}).

several minutes). BIP iron complexes with a single *ortho*-propenyl entity were prepared in the past, they are readily activated by MAO [58]. Apparently, a barrier exist for obtaining the MAO activated complex **1** when four propenyl moieties are in the ligand sphere.

TEA acts as expected as both an activator and chain transfer agent. Polymerization of ethylene at 3 bars of pressure in semi-batch gave catalyst activities in the range of 2–4 10^6 g.(mol Fe·bar·h)$^{-1}$ (Table 1). Although no specific screening for polymerization conditions was carried out, these conditions are generally useful for a controlled synthesis of polyethylenes with such BIP $FeCl_2$ complexes [57–59]. The polymer was isolated after the excess ethylene was discharged, and the reaction was quenched by the addition of small aliquots (5 – 20 mL) of ethanol. The products were dried in a temperature range below 40 °C to keep the product in a pristine state.

The bimodal distribution of the product shows polyethylene of low mass (~2 10^4 Da), resulting from chain transfer to aluminum with consecutive precipitation and UHMWPE (M_w of ~ 2·10^6 Da) [57]. Longer reaction times lead to more UHMWPE (Fig. 1). The formation of such high molecular weight polyethylene is not observed with BIP catalysts having only one propenyl entity per aniline in the ligand, not even at 10 bars of ethylene pressure. It is, however, found that the presence of propenyl entities enhances the molecular weight of the formed polyethylene, which is even more extensive in the catalysis with complex **1** [58].

Thus, the typical reactor blends of HDPE/UHMWPE were obtained with only one catalyst in form of **1** [9,16,60–62]. The ratio of HDPE to UMWPE would be adjustable by the reaction time or TEA concentration, however, this was not pursued here [63]. Whether the catalyst is incorporated into the polymer by an allylic insertion was also not the focus of this project, and was not addressed [58,64–66].

The DCSs show one melting isotherm, like is typical for in situ blends with single supports [49,67–69]. The thermal properties of the polymer are typical for not (fully) entangled UHMWPE [61]. The pristine material had a first (standard) melting point of 142.1 °C and a high degree of crystallinity of 73 % [27,70]. These properties were not restored after cooling the once molten sample from the molten state (Fig. 2). The second heating showed a material with melt temperature of 138.5 °C and the crystallinity decreased to 53 %. This behavior is in line with the loss of the disentangled state with its characteristic high crystalline content [24].

DSC-annealing experiments were carried out to investigate the disentangled state. These thermal experiments comprise an annealing step close to the melting point for a set time before a regular DSC-protocol with a heat rate of 10 °C.min^{-1} is executed (Table S1). The annealing temperature was a compromise of the second melting points of the samples after annealing at 137 °C (Table S1). The evolution of a secondary lower melting point is found with increasing annealing time. The lower peak corresponds to the melt crystalized material (~136 °C) while the higher melting peak (~140 °C) correspond to the nascent non-molten polymer crystals. Again, this is typical for melting of disentangled polyethylene, wherein lamellae detachment from nascent polymer crystals occurs. These detached chains can entangle and recrystallize upon cooling at a lower temperature [15,54]. Commercial entangled UHMWPE (GUR 4150–3: Mw: 8.1 10^6 g/mol and GUR 4012

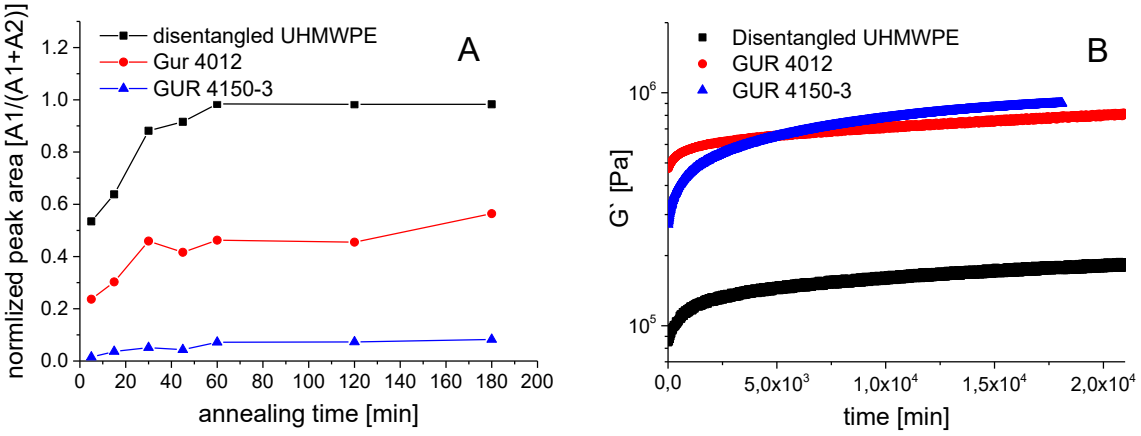

Fig. 3. A: Normalized peak area of the melting peaks from DSC annealing experiments with annealing time (left; A1: area at 136 °C, A2: at 141 °C); B: Development of the elastic modulus over time (right; 160 °C, 10 rad.s^{-1}, 0.2 % strain [54]).

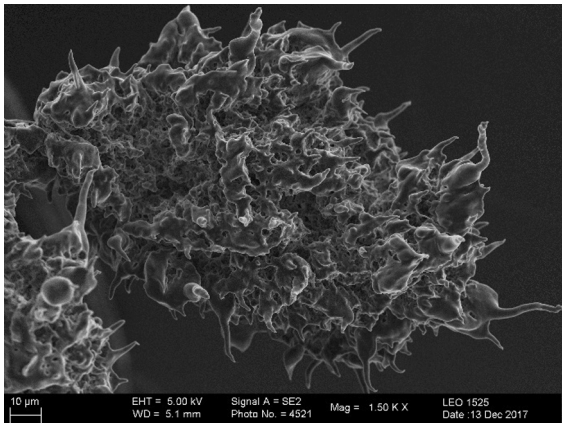

Fig. 4. SEM image of a nascent UHMWPE particle.

Mw: 1.7 10^6 g/mol) does not show this behavior to the same extent, and the time scale of detachment is longer as the higher amount of entanglements in the polymer crystals hinders the smooth and faster lamellae reorganization even in the sample of GUR 4012 with a similar molecular weight (Fig. 3**A**). A further indicator of the disentangled state of the polymer is that the characteristic elastic modulus G' increases in time upon first melting of a nascent polymer sample. The elastic modulus of the pristine dUHMWPE sample upon first melting is lower in the maiden state because of the molecular weight and fewer entanglements compared to commercial UHMWPE grades (Fig. 3**B**).

In addition, samples of blends pressed below the melting temperature (125 °C) into tapes [71] were well stretchable using the "hot shoe technique", while polymer samples pressed above the melting point (180 °C) appear quite brittle (**Figure S2**) [72]. The disentangled polymer chains in the cold-pressed sample slowly rearranged and aligned themselves in long fibers during the stretching procedure (**Figure S3**). The polymer chain segments in the hot-pressed sample could not slip past each other within the time frame of elongation, resulting an earlier mechanical failure.

3.2. Laser sintering of the dUHMWPE powder

The isolated powdery polymer showed no particular useful flowability, probably on account of the wide distribution of particle sizes and the irregular shapes and agglomerates. In addition, the surface of identified particle-like entities was not particular smooth (Fig. 4). The potential of the dUHMWPE blend for obtaining SLS built parts was nevertheless screened in a rudimentary experiment to obtain a proof of concept. One batch of isolated blend powder was therefore sieved to receive a sample that could be manipulated/flattened by the recoater of an EOSINT P 390 (EOS GmbH) SLS machine. Laser sintering at a temperature of the building chamber of 122 °C allowed fusion of the particles. A second layer could be applied and subsequent sintering gave essentially a 2D object with a geometry according to ISO 527–2 Type 5B (**Figure S2**).

The blend particles had fused together resulting in a shrinkage on account of a distinct melt flow of the low-density precursor (Fig. 5). The powder obviously had been completely molten in the focus of the laser beam (Fig. 5AB), and a substantial coalescence had taken place. This was taken as a promising observation for the approach of using disentangled particulate UHMWPE for the preparation of 3D objects by PBF/LB/P. Voids were regularly present, showing that the flow leading to densification and the concomitant increase of viscosity was too fast for the air to leave the sample. The low inherent density of the particles next to the anticipated loose packing of the spiky outside should also be improved. Non-molten particles adhered to the laser molten welded part, and some caking was observed (Fig. 5CD).

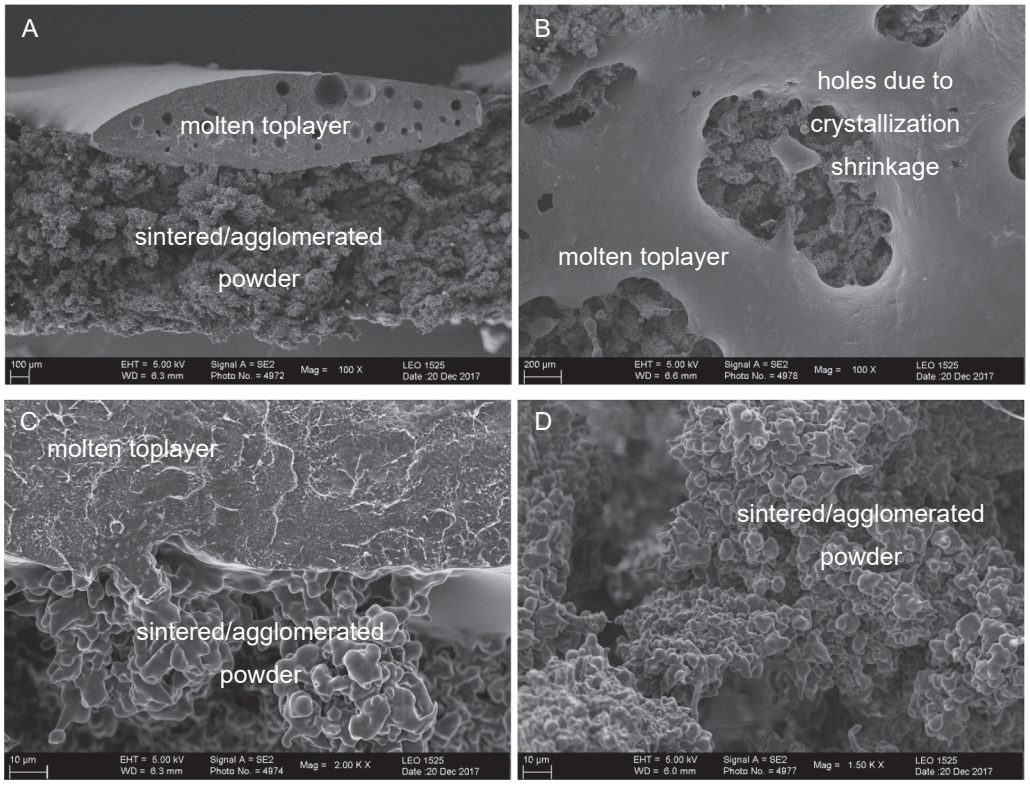

Fig. 5. SEM images of laser sintered dUMWPE/HDPE blends. A: Side view of cryo-fractured sample with a molten layer on top (100 x). B: Top view of laser sintered tensile specimen (100 x). C: Interface between molten layer and agglomerated particles (2 K x). D: Agglomerates beneath molten layer (1.5 K x).

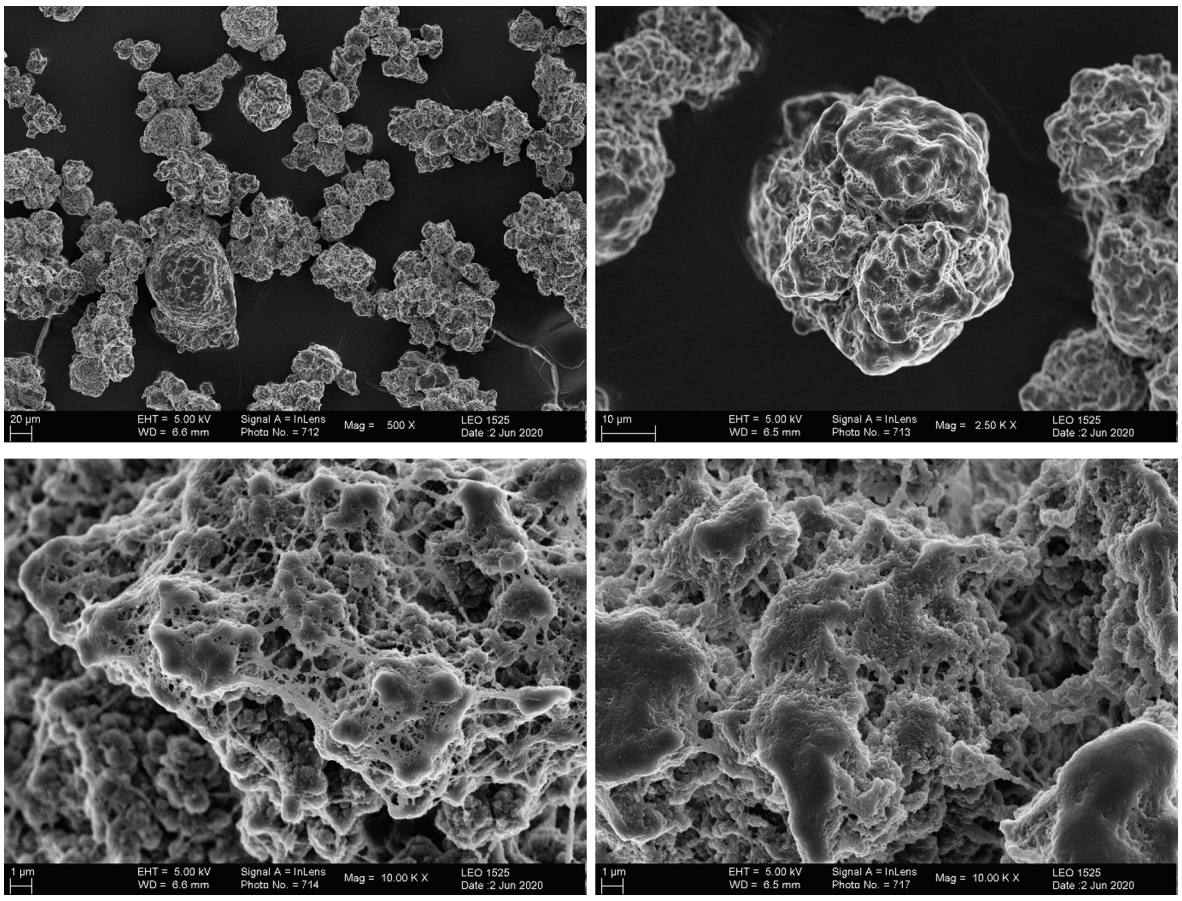

Fig. 6. SEM micrographs of dUHMWPE@silica synthesized with **1** supported on spray dried silica microparticles. Reaction conditions: 8 µmol.L^{-1} **1** on 1 g of spray dried silica microparticles, 9 mmol.L^{-1} TEA, 20 °C, 3 bar of ethylene, 200 RPM, 600 mL of toluene, 60 min.

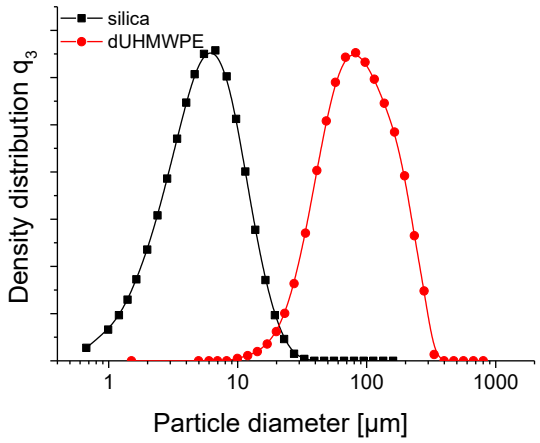

Fig. 7. Particle size distributions for dUHMWPE@silica particles. Reaction conditions: 8 µmol.L^{-1} **1** on 1 g of silica microparticles, 9 mmol.L^{-1} of TEA, 20 °C, 3 bar of ethylene, 200 RPM, 600 mL of toluene, 60 min of reaction time.

Table 2
Tensile properties of press sintered GUR UHMWPE and dUHMWPE samples.

	Yield stress [MPa]	Young modulus [MPa]	Ultimate tensile stress [MPa]	Elongation at break [%]
GUR 4150–3	16.8 ± 0.7	148 ± 38	44 ± 9	492 ± 65
dUHMWPE@silica	21.2 ± 0.5	156 ± 32	39 ± 11	450 ± 19

3.3. Silica template synthesis of HDPE/dUHMWPE blends

Next, a template synthesis of the polyethylene blend was targeted using a commercial available source of silica microparticles (in the following, dUHMWPE should be understood as the HDPE/dUHMWPE blend). It was found useful for obtaining more or less agglomerate free, spherical particle to redisperse the silica in water and re-isolate the particles by spray drying. The catalyst was applied molecularly to this support from a dichloro methane solution. A light blue, free-flowing powder was obtained after evaporating the solvent. The collected powder was dispersed in toluene and injected into a reactor charged with toluene and TEA. Prior to the addition of the catalyst, the toluene was saturated with ethylene at 3 bars of pressure. The reaction again was carried in semi-batch mode, now at 20 °C, continuously feeding ethylene to keep the pressure constant. The higher temperature was necessary for obtaining an acceptable activity.

A polyethylene shell was formed around the silica making up 96 % of the solid mass after 60 min. The resulting particles had an in essence spherical but somewhat irregular shape. Mostly individual particles are present, adhered into smaller, loose agglomerates (Fig. 6). The particles appear more compact than those prepared without a template, but still are porous and have a course surface. Individual lamellae are indicated in the SEM images. DLS analysis showed a more or less template copied particle size distribution with a median size of 85.5 ± 0.8 µm (Fig. 7). The shape of the distribution at the larger size range has a diffuse cut-off at about 200 µm, reminiscent of the presence of some agglomerates that do not breakup. The templating effect (replication) by the simple procedure thus was reasonably successful with respect to size and shape, but is also apt for improvement with respect to density and surface smoothness.

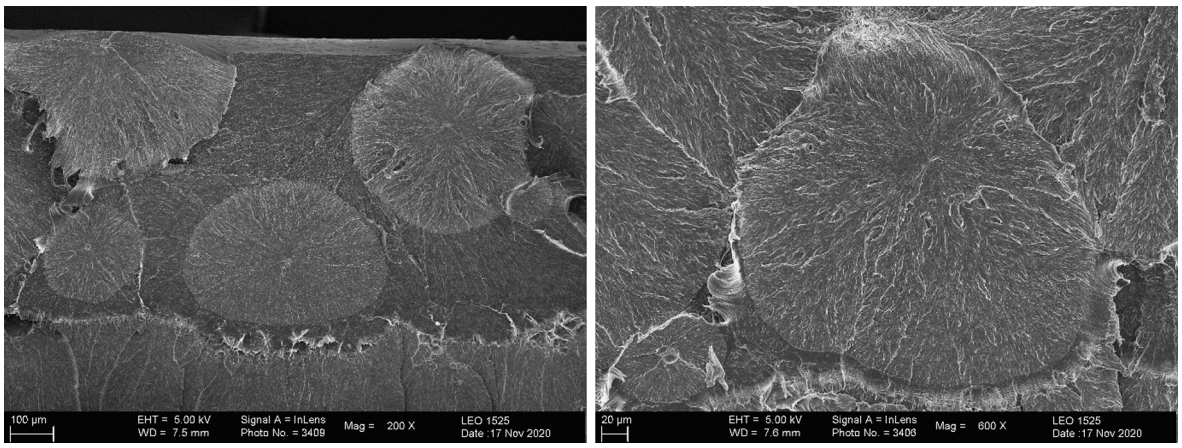

Fig. 8. SEM micrographs of a cryo-fractured press sintered dUHMWPE@silica sample with 3.9 wt% of silica.

3.4. Material properties of heat pressed dUHMWPE@silica

The tensile properties of thermal press sintered testing bars of the dUHMWPE@silica are in the range of similarly treated commercial UHMWPE (**Figure S4**; Table 2). Tensile test bars derived from DIN EN ISO 527-5A were manufactured by die cutting specimens from hot pressed plates. The stress strain behavior is the usual for a high molecular weight polyethylene with a yield point and strain hardening. Tensile testing of similarly processed commercial UHMWPE powder material (GUR 4150–3) with a very high molecular weight (M_v of $9*10^6$ Da) as benchmark showed a yield strength of 16.8 ± 0.7 MPa. It remains somewhat short of reported values (20 – 25 MPa) [73,74]. The formation of new entanglements may have needed more time [15]. The silica templated dUHMWPE based testing bar showed a higher yield point of up to 21.2 ± 0.5 MPa. The Young modulus, ultimate stress and elongation at break are somewhat lower than reported values, but statistically not different between the considered hot pressed materials (Table 2). The presence of 3.9 % of microsilica in the dUHMWPE blend and the lower molecular weight with a bimodal distribution may account for the differences in mean values.

Cryobreaking of the dUHMWPE@silica testing bar gives an even, flat breaking surface with no fiber pullouts. In contrast, the corresponding GUR UHMWPE sample shows a rough and uneven surface reminiscent of the originating particle conglomerate [75]. This shows that also in case of the template synthesis with **1**, disentangled (mobile) polyethylene is formed.

The structure of the press-sintered sample shows an unusual pattern with large crystallized spherical, spherulite like structures with clear boundaries (Fig. 8). The size of the structures is in the range of 200 – 400 µm. They possibly have a silica center as was concluded from the size of the recognizable higher density in the middle that is in the range of the parent silica particles. The spheres are embedded in apparently a more continuous matrix. The size of the structure reaches well-beyond that of the original particles; a complete reorganization of the polyethylene from the melt has taken place. These structures are not present in the heat pressed samples of commercial UHMWPE, their morphology shows a more granular structure at the size of originating particles (**Figure S5**) [75]. These new dUHMWPE particles thus may find use in procedures with thermal shaping to UHMWPE parts.

The onset of melting and crystallization of the dUHMWPE@silica is 129.8 resp. 119.3 °C, a laser sinter window results of about 10 °C. This is an even smaller value than for GUR 4150–3 of about 15 °C (**Table S3**), possibly originating from the nucleating action of the silica microparticulate template in combination with the HDPE part in dUHMWPE@silica [15]. A very accurate temperature control in SLS thus has become necessary [76].

The flowability of the dUHMWPE@silica has an fcc value of 3.44 in a ring shear tester. This number seemed too low for handling by a recoater in an SLS machine. Former experience with GUR 4150–3 had shown that processing in a speed mixer could improve the flowability of the powder. High energy impact on dUHMWPE@silica in a dual asymmetric centrifuge, however, led to a substantial decrease of the fcc value to 2.31. The sphericity was in the ~ 0.55 region and did not change much with high energy mixing, but the bulk density decreased by more than 1 unit (Table 3). The packing of the particles obviously became worse, possibly by an increase of edges, interlocking them and/or by the formation of fines. dUHMWPE crystallites may have been lost from the particles or from the agglomerates.

Table 3
Flow function, bulk density, and sphericity of dUHMWPE@silica.

source	ffc (500 Pa)	Bulk density [kg.m^{-3}]	Sphericity
as synthesized	3.44	130	0.55
after high energy mixing	2.31	115	0.54
additivition with 1 wt% silica & 0.25 wt % CB	2.59	72	0.58

The high energy treated dUHMWPE@silica particles were subsequently additivated with 1 wt% of nanosilica powder and 0.25 wt% of carbon black CB before screening in SLS. Nanosilica was used for its positive action on the flowability, which indeed restored some but not all of the flowability [5]. The CB was used for the low-density powder for absorbing reflected laser light. The addivation led even to a less dense powder with a density of 72 kg.m^{-3}. An optimization clearly is a project on its own, and will follow in the course of our current efforts after the parent UHMWPE@silica powder is further studied.

Despite the not too favorable properties of the dUHMWPE@silica

Fig. 9. Set of tensile test specimens of the type 1bb of dUHMWPE@silica with the addition of 1 wt% of nano silica and 0.25 wt% of CB built by PBF with the best practice parameters.

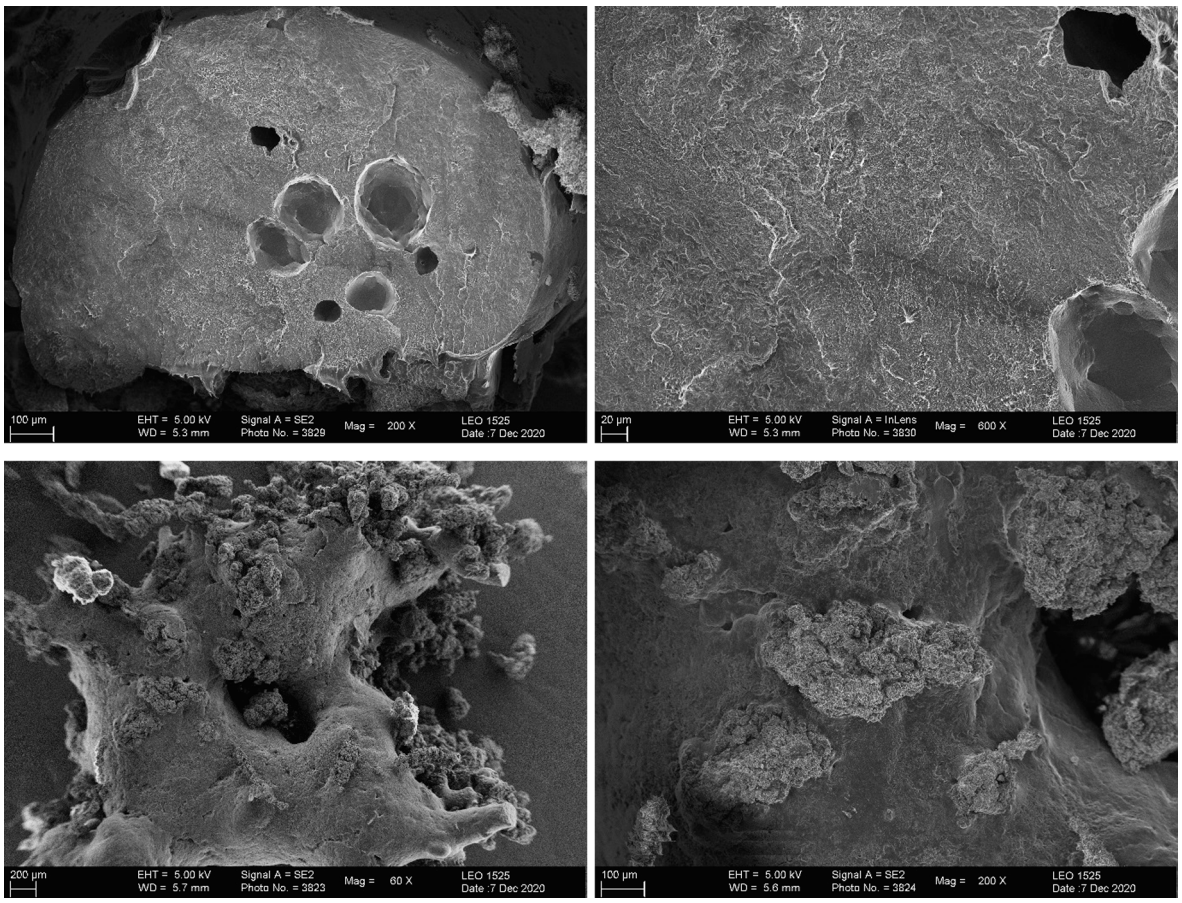

Fig. 10. SEM micrographs of the cryo-fractured tensile test specimens and its top surface of dUHMWPE with 1 wt% of nano silica and 0.25 wt% of CB built by PBF.

powders, orientating SLS experiments were performed. This was done also with the objective to assess the potential of the route for being useful in the preparation of UMWPE parts with properties close to those of bulk material. It was already clear, that several stages in the approach would need further attention. Initially found best practice parameters of a small study on printing HDPE powders were used in the operation of the printer. Latter study was performed in a miniaturized set up, allowing to sinter also research quantities of material [55].

Disappointingly, the built parts in form of testing bars showed a large amount of caking and could not be separated (Fig. 9). Scattering of laser light could not effectively be prevented by the added CB, leading to hardly recognizable printed testing bars. The low-density powder was taking up enough thermal energy to fully melt, inclusive its immediate surrounding. The surface of the built part, however, was very course and breaking the ensemble was easy. SEM micrographs revealed that the structure of the intended testing bars consisted of few consolidated droplets of polymer melt but a solid part had not formed (Fig. 10). The very low bulk density of the powder may be the cause for this. The break surface of such a droplet was clean and even with few pores, indicating again a good welding. These results display the general possibility of manufacturing parts of dUHMWPE with a PBF process. However, the bulk density of the powders needs to be increased. Current research is directed toward this.

4. Conclusions

A new BIP iron(II) catalyst was discovered that is activated by TEA to give a blend of HDPE and substantially disentangled UHMWPE. Laser sintering of the material is possible and the result indicated that a good welding is possible, i.e. a low viscous melt can be generated that fuses to a solid 2D object with some voids. The complex can be supported on micro-sized silica to give a template for HDPE/dUHMWPE@silica particles in a range below 200 µm. Thermal sintering of the powder gives a material with typical UHMWPE properties. The morphology shows that the powder has been fully molten and a crystallization initiated from the silica particles gives an unusual internal structure. The sphericity and flow properties of the dUHMWPE@silica are promising, however, the particles need optimization with respect to density and packing for making them more suitable for 3D printing along PBF/LB/P.

CRediT authorship contribution statement

Yannick L. Wencke: Investigation, Formal analysis, Writing – original draft, Visualization. **Gerrit A. Luinstra:** Funding acquisition, Conceptualization, Writing – review & editing, Supervision. **Rob Duchateau:** Writing – review & editing. **Friedrich Proes:** Investigation, Writing – review & editing. **Philipp Imgrund:** Project administration. **Jonathan S. Evenson:** Investigation. **Claus Emmelmann:** Funding acquisition, Supervision.

Declaration of Competing Interest

The authors declare that they have no known competing financial interests or personal relationships that could have appeared to influence the work reported in this paper.

Acknowledgements

The supporting and SLS experimenting was within the DFG funded priority program SPP2122 Materials for Additive Manufacturing (Lu 620/3-1 and EM 95/6-1), should read: The catalyst supporting chemistry and SLS experimenting was within the DFG funded priority

program SPP2122 Materials for Additive Manufacturing (Lu 620/3-1 and EM 95/6-1).

Appendix A. Supplementary material

Supplementary data to this article can be found online at https://doi.org/10.1016/j.eurpolymj.2021.110936.

References

[1] K. Patel, S.H. Chikkali, S. Sivaram, Ultrahigh molecular weight polyethylene: Catalysis, structure, properties, processing and applications, Prog. Polym. Sci. 109 (2020) 101290, https://doi.org/10.1016/j.progpolymsci.2020.101290.

[2] S.M. Kurtz (Ed.), UHMWPE biomaterials handbook: Ultra high molecular weight polyethylene in total joint replacement and medical devices, William Andrew an imprint of Elsevier, Amsterdam, Boston, (2016).

[3] S. Changhui, H. Aibing, Y. Yongqiang, W. Di, Y.u. Jia-kuo, Customized UHMWPE tibial insert directly fabricated by selective laser sintering, Int. J. Adv. Manuf. Technol. 85 (5-8) (2016) 1217–1226, https://doi.org/10.1007/s00170-015-8046-6.

[4] R.D. Goodridge, R.J.M. Hague, C.J. Tuck, An empirical study into laser sintering of ultra-high molecular weight polyethylene (UHMWPE), J. Mater. Process. Technol. 210 (1) (2010) 72–80, https://doi.org/10.1016/j.jmatprotec.2009.08.016.

[5] X. Zhu, Q.i. Yang, Sintering the feasibility improvement and mechanical property of UHMWPE via selective laser sintering, Plast. Rubber Compos. 49 (3) (2020) 116–126, https://doi.org/10.1080/14658011.2020.1718321.

[6] Y. Khalil, N. Hopkinson, A. Kowalski, J.P.A. Fairclough, Characterisation of UHMWPE polymer powder for laser sintering, Materials 12 (2019) 3496, https://doi.org/10.3390/ma12213496.

[7] C.A. Chatham, T.E. Long, C.B. Williams, A review of the process physics and material screening methods for polymer powder bed fusion additive manufacturing, Prog. Polym. Sci. 93 (2019) 68–95, https://doi.org/10.1016/j.progpolymsci.2019.03.003.

[8] R. Brighenti, M.P. Cosma, L. Marsavina, A. Spagnoli, M. Terzano, Laser-based additively manufactured polymers: a review on processes and mechanical models, J. Mater. Sci. 56 (2) (2021) 961–998, https://doi.org/10.1007/s10853-020-05254-6.

[9] M. Stürzel, S. Mihan, R. Mülhaupt, From Multisite Polymerization Catalysis to Sustainable Materials and All-Polyolefin Composites, Chem. Rev. 116 (3) (2016) 1398–1433, https://doi.org/10.1021/acs.chemrev.5b00310.

[10] H. Scholten, W. Christoph, Use of a polyamide 12 for selective laser sintering. CAPLUS AN 1999:279704(Patent), Eur. Pat. Appl. Copyright © 2021 American Chemical Society (ACS). All Rights Reserved 7 pp.

[11] C.T. Bellehumeur, M.K. Bisaria, J. Vlachopoulos, An experimental study and model assessment of polymer sintering, Polym. Eng. Sci. 36 (17) (1996) 2198–2207, https://doi.org/10.1002/pen.10617.

[12] Y. Khalil, A. Kowalski, N. Hopkinson, Influence of laser power on tensile properties and material characteristics of laser-sintered UHMWPE, Manuf. Rev. 3 (2016) 15/1-15/9, https://doi.org/10.1051/mfreview/2016015.

[13] J.T. Rimell, P.M. Marquis, Selective laser sintering of ultra high molecular weight polyethylene for clinical applications, J. Biomed. Mater. Res. 53 (2000) 414–420, https://doi.org/10.1002/1097-4636(2000)53:4<414:AID-JBM16>3.0.CO;2-M.

[14] A. Galeski, M. Psarski, Morphology and kinetics of crystallization of polyethylene from chain disentangled melt, Macromol. Symp. 104 (1) (1996) 183–190, https://doi.org/10.1002/masy.19961040118.

[15] T. Deplancke, O. Lame, F. Rousset, I. Aguili, R. Seguela, G. Vigier, Diffusion versus Cocrystallization of Very Long Polymer Chains at Interfaces: Experimental Study of Sintering of UHMWPE Nascent Powder, Macromolecules (Washington, DC, U. S.) 47 (2014) 197–207. https://doi.org/10.1021/ma402012f.

[16] D. Hofmann, A. Kurek, R. Thomann, J. Schwabe, S. Mark, M. Enders, T. Hees, R. Mülhaupt, Tailored Nanostructured HDPE Wax/UHMWPE Reactor Blends as Additives for Melt-Processable All-Polyethylene Composites and in Situ UHMWPE Fiber Reinforcement, Macromolecules (Washington, DC, U. S.) 50 (2017) 8129–8139. https://doi.org/10.1021/acs.macromol.7b01891.

[17] M. Rezaei, N.G. Ebrahimi, M. Kontopoulou, Thermal properties, rheology and sintering of ultra high molecular weight polyethylene and its composites with polyethylene terephthalate, Polym. Eng. Sci. 45 (5) (2005) 678–686, https://doi.org/10.1002/pen.20319.

[18] D. Romano, S. Ronca, S. Rastogi, A hemi-metallocene chromium catalyst with trimethylaluminum-free methylaluminoxane for the synthesis of disentangled ultra-high molecular weight polyethylene, Macromol. Rapid Commun. 36 (3) (2015) 327–331, https://doi.org/10.1002/marc.201400514.

[19] I.V. Oleynik, I.K. Shundrina, I.I. Oleyinik, Highly active titanium(IV) dichloride FI catalysts bearing a diallylamino group for the synthesis of disentangled UHMWPE, Polym. Adv. Technol. 31 (2020) 1921–1934, https://doi.org/10.1002/pat.4917.

[20] A. Heidari, H. Zarghami, S. Talebi, M. Rezaei, A disentangled state using TiCl4/MgCl2 catalyst: a case study of polyethylene, Iran, Polym. J. 27 (9) (2018) 701–708, https://doi.org/10.1007/s13726-018-0648-z.

[21] A. Pandey, Y. Champouret, S. Rastogi, Heterogeneity in the Distribution of Entanglement Density during Polymerization in Disentangled Ultrahigh Molecular Weight Polyethylene, Macromolecules (Washington, DC, U. S.) 44 (2011) 4952–4960. https://doi.org/10.1021/ma2003689.

[22] G. Forte, S. Ronca, Synthesis of Disentangled Ultra-High Molecular Weight Polyethylene: Influence of Reaction Medium on Material Properties, Int. J. Polym. Sci. 2017 (2017) 1–8, https://doi.org/10.1155/2017/7431419.

[23] A. Petrov, V.Y. Rudyak, P. Kos, A. Chertovich, Polymerization of Low-Entangled Ultrahigh Molecular Weight Polyethylene: Analytical Model and Computer Simulations, Macromolecules (Washington, DC, U. S.) 53 (2020) 6796–6808. https://doi.org/10.1021/acs.macromol.0c01077.

[24] R.P. Gote, D. Mandal, K. Patel, K. Chaudhuri, C.P. Vinod, A.K. Lele, S.H. Chikkali, Judicious Reduction of Supported Ti Catalyst Enables Access to Disentangled Ultrahigh Molecular Weight Polyethylene, Macromolecules (Washington, DC, U. S.) 51 (2018) 4541–4552. https://doi.org/10.1021/acs.macromol.8b00590.

[25] Z. Yue, N. Wang, Y.u. Cao, W. Li, C.-D. Dong, Reduced Entanglement Density of Ultrahigh-Molecular-Weight Polyethylene Favored by the Isolated Immobilization on the MgCl 2 (110) Plane, Ind. Eng. Chem. Res. 59 (8) (2020) 3351–3358, https://doi.org/10.1021/acs.iecr.9b06780.

[26] P. Chen, H. Yang, T. Chen, W. Li, Weakly Entangled Ultrahigh Molecular Weight Polyethylene Prepared via Ethylene Extrusion Polymerization, Ind. Eng. Chem. Res. 54 (44) (2015) 11024–11032, https://doi.org/10.1021/acs.iecr.5b03059.

[27] D. Romano, N. Tops, E. Andablo-Reyes, S. Ronca, S. Rastogi, Influence of Polymerization Conditions on Melting Kinetics of Low Entangled UHMWPE and Its Implications on Mechanical Properties, Macromolecules (Washington, DC, U. S.) 47 (2014) 4750–4760. https://doi.org/10.1021/ma5008122.

[28] F.P. Wimmer, V. Ebel, F. Schmidt, S. Mecking, Compartmentalized polymerization in aqueous and organic media to low-entangled ultra high molecular weight polyethylene, Polym. Chem. 12 (21) (2021) 3116–3123, https://doi.org/10.1039/D1PY00394A.

[29] S. Rastogi, L. Kurelec, J. Cuijpers, D. Lippits, M. Wimmer, P.J. Lemstra, Disentangled State in Polymer Melts; a Route to Ultimate Physical and Mechanical Properties, Macromol. Mater. Eng. 288 (12) (2003) 964–970, https://doi.org/10.1002/mame.200300113.

[30] H. Xu, C.-Y. Guo, Polymerization in the confinement of molecular sieves: Facile preparation of high performance polyethylene, Eur. Polym. J. 65 (2015) 15–32, https://doi.org/10.1016/j.eurpolymj.2014.11.037.

[31] P. Kenyon, S. Mecking, Pentafluorosulfanyl Substituents in Polymerization Catalysis, J. Am. Chem. Soc. 139 (39) (2017) 13786–13790, https://doi.org/10.1021/jacs.7b06745.

[32] W. Li, T. Chen, C. Guan, D. Gong, J. Mu, Z.-R. Chen, Q.i. Zhou, Influence of Polyhedral Oligomeric Silsesquioxane Structure on the Disentangled State of Ultrahigh Molecular Weight Polyethylene Nanocomposites during Ethylene in Situ Polymerization, Ind. Eng. Chem. Res. 54 (5) (2015) 1478–1486, https://doi.org/10.1021/ie504273r.

[33] W. Li, C. Guan, J. Xu, Z.-R. Chen, B. Jiang, J. Wang, Y. Yang, Bimodal/Broad Polyethylene Prepared in a Disentangled State, Ind. Eng. Chem. Res. 53 (3) (2014) 1088–1096, https://doi.org/10.1021/ie403315v.

[34] W. Li, H. Yang, M. Shang, T. Chen, W. Wang, Structural and Morphological Evolution of Nascent Polyethylene during Ethylene in Situ Polymerization within Fe 3 O 4 @SiO 2 Nanoparticles, Ind. Eng. Chem. Res. 55 (32) (2016) 8719–8725, https://doi.org/10.1021/acs.iecr.6b01312.

[35] R. Bärenwald, S. Goerlitz, R. Godehardt, A. Osichow, Q. Tong, M. Krumova, S. Mecking, K. Saalwächter, Local Flips and Chain Motion in Polyethylene Crystallites: A Comparison of Melt-Crystallized Samples, Reactor Powders, and Nanocrystals, Macromolecules (Washington, DC, U. S.) 47 (2014) 5163–5173. https://doi.org/10.1021/ma500691k.

[36] P. Chammingkwan, Y. Bando, L.T.T. Mai, T. Wada, A. Thakur, M. Terano, L. Sinthusai, T. Taniike, Less Entangled Ultrahigh-Molecular-Weight Polyethylene Produced by Nano-Dispersed Ziegler-Natta Catalyst, Ind. Eng. Chem. Res. 60 (7) (2021) 2818–2827, https://doi.org/10.1021/acs.iecr.0c05432.

[37] R. Huang, C.E. Koning, J.C. Chadwick, Synergetic Effect of a Nickel Diimine in Ethylene Polymerization with Immobilized Fe-, Cr-, and Ti-Based Catalysts on MgCl 2 Supports, Macromolecules (Washington, DC, U. S.) 40 (2007) 3021–3029. https://doi.org/10.1021/ma070071j.

[38] R. Hoff, Handbook of Transition Metal Polymerization Catalysts, secondnd ed., John Wiley & Sons Incorporated, Newark, 2018.

[39] M. Chen, Y. Chen, W. Li, P. Liang, C. Ren, B. Jiang, J. Wang, Y. Yang, Synthesis of Weakly Entangled Ultra-High-Molecular-Weight Polyethylene with a Fine Particle Size, Ind. Eng. Chem. Res. 60 (8) (2021) 3354–3362, https://doi.org/10.1021/acs.iecr.0c05838.

[40] W. Zhang, W.-H. Sun, C. Redshaw, Tailoring iron complexes for ethylene oligomerization and/or polymerization, Dalton Trans. 42 (25) (2013) 8988–8997, https://doi.org/10.1039/C2DT32337K.

[41] Y. Champouret, O.H. Hashmi, M. Visseaux, Discrete iron-based complexes: Applications in homogeneous coordination-insertion polymerization catalysis, Coord. Chem. Rev. 390 (2019) 127–170, https://doi.org/10.1016/j.ccr.2019.03.015.

[42] V.A. Zakharov, N.V. Semikolenova, T.B. Mikenas, A.A. Barabanov, G.D. Bukatov, L. G. Echevskaya, M.A. Mats'ko, Homogeneous and supported catalysts based on bis (imino)pyridyl Iron(II) complexes for ethylene polymerization, Kinet Catal 47 (2006) 303–309. https://doi.org/10.1134/S0023158406020236.

[43] A.A. Barabanov, G.D. Bukatov, V.A. Zakharov, N.V. Semikolenova, T.B. Mikenas, L. G. Echevskaja, M.A. Matsko, Kinetic Study of Ethylene Polymerization Over Supported Bis(imino)pyridine Iron (II) Catalysts, Macromol. Chem. Phys. 207 (15) (2006) 1368–1375, https://doi.org/10.1002/macp.200600122.

[44] R. Huang, N. Kukalyekar, C.E. Koning, J.C. Chadwick, Immobilization and activation of 2,6-bis(imino)pyridyl Fe, Cr and V precatalysts using a MgCl2/AlRn (OEt)3−n support: Effects on polyethylene molecular weight and molecular weight

distribution, J. Mol. Catal. A: Chem. 260 (1-2) (2006) 135–143, https://doi.org/10.1016/j.molcata.2006.07.030.
[45] S. Ray, S. Sivaram, Silica-supported bis(imino)pyridyl iron(II) catalyst: nature of the support–catalyst interactions, Polym. Int. 55 (8) (2006) 854–861, https://doi.org/10.1002/pi.2020.
[46] N.V. Semikolenova, V.N. Panchenko, E.A. Paukshtis, M.A. Matsko, V.A. Zakharov, Study of supported catalysts, prepared via binding of Fe(II) bis(imino)pyridyl complex with silica, modified by alumina: Effect of surface Lewis acidic sites on catalyst composition and activity in ethylene polymerization, Mol. Catal. 486 (2020) 110878, https://doi.org/10.1016/j.mcat.2020.110878.
[47] E. Bauer (Ed.), Iron Catalysis II, Springer International Publishing, Cham, 2015.
[48] S.B. Cordeiro, M.d.F.V. Marques, Evaluation of Bis(imino)pyridine Iron Catalyst on Heterogeneous Ethylene Polymerization, Ch&Cht 14 (2) (2020) 185–194.
[49] H. Liu, E.M. Troisi, J.G.P. Goossens, J.R. Severn, C.W.M. Bastiaansen, Rheological properties of bimodal polyethylenes produced with silica nanoparticle supported catalysts, J. Appl. Polym. Sci. 136 (21) (2019) 47577, https://doi.org/10.1002/app.v136.2110.1002/app.47577.
[50] N. Kukalyekar, L. Balzano, G.W.M. Peters, S. Rastogi, J.C. Chadwick, Characteristics of Bimodal Polyethylene Prepared via Co-Immobilization of Chromium and Iron Catalysts on an MgCl 2 -Based Support, Macromol. React. Eng. 3 (8) (2009) 448–454, https://doi.org/10.1002/mren.200900021.
[51] H.-W. Shen, B.-H. Xie, W. Yang, M.-B. Yang, Thermal and rheological properties of polyethylene blends with bimodal molecular weight distribution, J Appl Polym Sci 129 (4) (2013) 2145–2151, https://doi.org/10.1002/app.v129.410.1002/app.38850.
[52] J.R. Severn, J.C. Chadwick, Tailor-Made Polymers, Wiley, 2008.
[53] H.L. Wagner, The Mark–Houwink–Sakurada Equation for the Viscosity of Linear Polyethylene, J. Phys. Chem. Ref. Data 14 (2) (1985) 611–617, https://doi.org/10.1063/1.555751.
[54] M. Spronck, A. Klein, B. Blom, D. Romano, Synthesis of Disentangled Ultra-High Molecular Weight Polyethylene using Vanadium(V)-Based Catalysts, Z. Anorg. Allg. Chem. 644 (17) (2018) 993–998, https://doi.org/10.1002/zaac.201800165.
[55] J.S. Evenson, Y.L. Wencke, G.A. Luinstra, C. Emmelmann, in: B. Müller (Ed.), Fraunhofer Direct Digital Manufacturing Conference DDMC 2020: Conference Proceedings, March 2020, Berlin, Germany, Fraunhofer Verlag, Stuttgart, 2020.
[56] S. Kotha, V.R. Shah, Design and Synthesis of 1-Benzazepine Derivatives by Strategic Utilization of Suzuki-Miyaura Cross-Coupling, Aza-Claisen Rearrangement and Ring-Closing Metathesis, Eur. J. Org. Chem. 2008 (6) (2008) 1054–1064, https://doi.org/10.1002/ejoc.200700921.
[57] E.M. Schoeneberger, G.A. Luinstra, Investigations on the Ethylene Polymerization with Bisarylimine Pyridine Iron (BIP) Catalysts, Catalysts 11 (2021) 407, https://doi.org/10.3390/catal11030407.
[58] C. Görl, H.G. Alt, Iron complexes with ω-alkenyl substituted bis(arylimino)pyridine ligands as catalyst precursors for the oligomerization and polymerization of ethylene, J. Mol. Catal. A: Chem. 273 (1-2) (2007) 118–132, https://doi.org/10.1016/j.molcata.2007.04.001.
[59] V.C. Gibson, G.A. Solan, Olefin Oligomerizations and Polymerizations Catalyzed by Iron and Cobalt Complexes Bearing Bis(imino)pyridine Ligands, in: R.M. Bullock (Ed.), Catalysis without Precious Metals, Wiley-VCH Verlag GmbH & Co. KGaA, Weinheim, Germany, 2010, pp. 111–141.
[60] Z. Yang, J. Shi, X. Pan, B. Liu, X. He, Effects of different ultrahigh molecular weight polyethylene contents on the formation and evolution of hierarchical crystal structure of high-density polyethylene/ultrahigh molecular weight polyethylene blend fibers, J. Polym. Sci. 58 (16) (2020) 2278–2291, https://doi.org/10.1002/pol.20200205.
[61] F. Zhong, R. Thomann, R. Mülhaupt, Tailoring Mono-, Bi-, and Trimodal Molar Mass Distributions and All-Hydrocarbon Composites by Ethylene Polymerization on Bis(imino)pyridine Chromium(III) Supported on Ultrathin Gibbsite Single Crystal Nanoplatelets, Macromolecules (Washington, DC, U. S.) 52 (2019) 2701–2711. https://doi.org/10.1021/acs.macromol.9b00091.
[62] A.E. Ferreira, M.L. Cerrada, E. Perez, V. Lorenzo, E. Valles, J. Ressia, H. Cramail, J. P. Lourenco, M.R. Ribeiro, UHMWPE/HDPE in-reactor blends, prepared by in situ polymerization: Synthetic aspects and characterization, Express Polym. Lett. 11 (2017) 344–361. https://doi.org/10.3144/expresspolymlett.2017.34.
[63] A. Valente, A. Mortreux, M. Visseaux, P. Zinck, Coordinative chain transfer polymerization, Chem. Rev. 113 (5) (2013) 3836–3857, https://doi.org/10.1021/cr300289z.
[64] M. Seitz, W. Milius, H.G. Alt, Iron(II) coordination compounds with ω-alkenyl substituted bis(imino)pyridine ligands: Self-immobilizing catalysts for the polymerization of ethylene, J. Mol. Catal. A: Chem. 261 (2) (2007) 246–253, https://doi.org/10.1016/j.molcata.2006.07.078.
[65] H. Alshammari, H.G. Alt, Transition Metal Complexes of Allylated α-Diimines as Self-Immobilizing Catalysts for the Polymerization of Ethylene, JJC 9 (2014) 34–49, https://doi.org/10.12816/0026393.
[66] H.G. Alt, C. Grl, Self-Immobilizing Catalysts for Olefin Polymerization, in: J. R. Severn, J.C. Chadwick (Eds.), Tailor-Made Polymers, Wiley-VCH Verlag GmbH & Co. KGaA, Weinheim, Germany, 2008, pp. 305–326.
[67] Z. Wang, G.A. Solan, W. Zhang, W.-H. Sun, Carbocyclic-fused N, N, N-pincer ligands as ring-strain adjustable supports for iron and cobalt catalysts in ethylene oligo-/polymerization, Coord. Chem. Rev. 363 (2018) 92–108, https://doi.org/10.1016/j.ccr.2018.02.016.
[68] M. Chen, Y. Chen, W. Li, C. Dong, P. Liang, N. Wang, B. Jiang, J. Wang, Y. Yang, Selective distribution and contribution of nickel based pre-catalyst in the multisite catalyst for the synthesis of desirable bimodal polyethylene, Eur. Polym. J. 135 (2020), 109878, https://doi.org/10.1016/j.eurpolymj.2020.109878.
[69] H. Liu, C.W.M. Bastiaansen, J.G.P. Goossens, A.P.H.J. Schenning, J.R. Severn, Bimodal Ultrahigh Molecular Weight Polyethylenes Produced from Supported Catalysts: The Challenge of Using a Combined Catalyst System, Macromol. Chem. Phys. 218 (2017) 1600490, https://doi.org/10.1002/macp.201600490.
[70] B. Wunderlich, Thermal Analysis of Polymeric Materials, Springer-Verlag Berlin Heidelberg, Berlin, Heidelberg, 2005.
[71] S. Rastogi, Y. Yao, S. Ronca, J. Bos, J. van der Eem, Unprecedented High-Modulus High-Strength Tapes and Films of Ultrahigh Molecular Weight Polyethylene via Solvent-Free Route, Macromolecules (Washington, DC, U. S.) 44 (2011) 5558–5568. https://doi.org/10.1021/ma200667m.
[72] Rastogi, Kurelec, Lemstra, Chain Mobility in Polymer Systems: On the Borderline between Solid and Melt. 2. Crystal Size Influence in Phase Transition and Sintering of Ultrahigh Molecular Weight Polyethylene via the Mobile Hexagonal Phase, Macromolecules (Washington, DC, U. S.) 31 (1998) 5022–5031. https://doi.org/10.1021/ma980261h.
[73] L. Fang, Y. Leng, P. Gao, Processing and mechanical properties of HA/UHMWPE nanocomposites, Biomaterials 27 (2006) 3701–3707, https://doi.org/10.1016/j.biomaterials.2006.02.023.
[74] A. Bistolfi, M.B. Turell, Y.-L. Lee, A. Bellare, Tensile and tribological properties of high-crystallinity radiation crosslinked UHMWPE, J. Biomed. Mater. Res. B Appl. Biomater. 90 (2009) 137–144, https://doi.org/10.1002/jbm.b.31265.
[75] R. Hosseinnezhad, S. Talebi, M. Rezaei, The unique effect of chain entanglements and particle morphology on the sintering of ultrahigh molecular weight polyethylene, J. Elastomers Plast. 49 (2017) 609–629, https://doi.org/10.1177/0095244316681833.
[76] M. Schmid, Laser sintering with plastics: Technology, processes, and materials, Carl Hanser Verlag, Munich, 2018.